Schweizerische Eidgenossenschaft
Confédération suisse
Confederazione Svizzera
Confederaziun svizra

Federal Department of the
Environment, Traffic, Energy and Communications DETEC

Swiss Federal Office of Energy

Final report 31.12.2014

PECHouse2

Photoelectrochemical water splitting for solar production of hydrogen

Contracting body:

Swiss Federal Office of Energy SFOE
Research Programme XY
CH-3003 Bern
www.bfe.admin.ch

Authors:

Matthew T. Mayer, EPFL, matthew.mayer@epfl.ch
Michael Graetzel, EPFL, michael.graetzel@epfl.ch
Peter Cendula, ZHAW, cend@zhaw.ch
Jürgen Schumacher, ZHAW, schm@zhaw.ch

SFOE Head of domain: Stefan Oberholzer
SFOE Programme manager: Stefan Oberholzer
SFOE Contract number: BFE-1081-00224

The authors only are responsible for the content and the conclusions of this report.

Zusammenfassung

Photoelektroden für wasserspaltende Solarzellen aus häufig vorkommenden Materialien werden im Labor für Photonik und Grenzflächen an der EPF Lausanne entwickelt. Im Projekt PECHouse2 untersuchten wir Metalloxid-Photoelektroden aus Eisenoxid und Kupferoxid und zusätzlich auch neue Hochleistungswerkstoffe zur photoelektrochemischen (PEC) Wasserspaltung. Wasserstoffproduktion aus Sonnenlicht konnte in verschiedenen Konfigurationen der Zellkomponenten realisiert werden. Ausserdem wurden wichtige Schritte in Richtung einer Marktfähigkeit der Technologie unternommen. Am Institute of Computational Physics der ZHAW wird an einem Verständnis der physikalischen Prozesse und deren Optimierung für die effiziente solare Wasserspaltung gearbeitet. Mit einem im Projekt entwickelten elektrischen Modell wurden numerische Simulationen von Eisenoxid und Kupferoxid Photoelektroden durchgeführt. Die Bandlückenenergie wurde variiert, Strom-Spannungskennlinien berechnet und Impedanzspektren simuliert. Durch eine spektral aufgelöste optische Charakterisierung und Modellierung gelang es uns alle optischen Verlustkanäle für Eisenoxid zu bestimmen.

Résumé

Photoélectrodes pour décomposition de l'eau axée sur la lumière du soleil en utilisant des matériaux peu coûteux et abondants sont développés au Laboratoire de photonique et interfaces à l'EPFL. Dans PECHouse2 nous avancions photoélectrodes d'oxyde métalliques terre abondante base d'oxyde de fer et l'oxyde cuivreux vers photoélectrochimiques applications (PEC) de décomposition de l'eau, en plus de poursuivre un certain nombre de nouveaux matériaux de haute performance. Nous avons réalisé sans aide décomposition de l'eau axée sur la lumière du soleil dans plusieurs configurations de périphériques différents, avancer plus loin la technologie vers la viabilité commerciale. Compréhension théorique des processus physiques sous-jacents et leur optimisation pour le fractionnement efficace de l'eau solaire est à l'étude à l'Institut de Physique, ZHAW. Simulations numériques basées sur notre modèle électrique ont aidé à comprendre l'alignement de bande énergétique de l'oxyde de fer et photoélectrodes d'oxyde cuivreux et leur réponse photocourant-tension. Modèles électriques avec transfert de charge à partir de la bande de valence ou des états de surface, un sujet controversé discuté dans la littérature récente, ont été comparées par la réponse de la spectroscopie d'impédance. Caractérisation optique détaillée et la modélisation nous a permis de résoudre spectralement tous les canaux de perte optiques pour l'oxyde de fer.

Abstract

Photoelectrodes for solar water splitting utilizing cheap and abundant materials are being developed at the Laboratory of Photonics and Interfaces at EPFL. In PECHouse2 we advanced earth-abundant metal oxide photoelectrodes based on iron oxide and cuprous oxide toward photoelectrochemical (PEC) water splitting applications, in addition to pursuing a number of new high-performance materials. We achieved unassisted sunlight-driven water splitting in several different device configurations, further advancing the technology toward commercial viability. Theoretical understanding of the underlying physical processes and their optimization for efficient solar water splitting is being studied at the Institute of Computational Physics, ZHAW. Numerical simulations based on our electrical model helped to understand energetic band alignment of iron oxide and cuprous oxide photoelectrodes and their photocurrent-voltage response. Electrical models with charge transfer from valence band or surface states, a controversial topic discussed in the recent literature, were compared by impedance spectroscopy response. Detailed optical characterization and modeling allowed us to spectrally resolve all optical loss channels for iron oxide.

PECHouse2

Final Report

January 2015

Laboratory of Photonics and Interfaces, EPFL

Institute of Computational Physics, ZHAW

Initial position (context, starting point)

The PECHouse2 project began in 2012 following the completion of the original PECHouse project. Initiated in 2007, PECHouse was established as the photoelectrochemistry (PEC) centre of competence at the Swiss Federal Institute of Technology of Lausanne (EPFL) with the goal of advancing semiconductor-based photoelectrochemical water splitting to produce H_2. The project achieved breakthroughs in performance for metal oxide photocathodes and photoanodes, while also increasing the fundamental understanding in the research field. Concurrently, the EU FP7 project NanoPEC represented an international effort to further the development of materials toward PEC application.

Goal of the project

The PECHouse2 project aimed to advance the findings of PECHouse toward real demonstrations of solar-to-H_2 conversion together with model-based characterizations of the electrodes. Focusing largely on electrodes based on iron oxide (Fe_2O_3) and copper oxide (Cu_2O), we aimed to increase their performances in terms of photocurrent and photovoltage. We sought to study the degradation processes and device approaches to increasing the stability of water splitting photoelectrodes. We worked to develop numerical models for the operation of a PEC cell, integrate them into a computer program, and use the model to understand the operation of actual electrodes and to predict the optimized device design. Finally, we aimed to demonstrate the concepts of materials and device design in the form of a scaled-up demonstrator device capable of unassisted water splitting.

Procedure / method

A variety of methods were used to develop and study the photoelectrode devices. Photocathodes were synthesized by electrodeposition of Cu_2O onto Au-covered FTO/glass substrates, followed by atomic layer deposition (ALD) of overlayers, as previously described.[1] New overlayers and catalyst treatments were developed in PECHouse2, as described in the Results section. Photoanodes based on Fe_2O_3 were synthesized by the atmospheric pressure chemical vapor deposition (APCVD) or ultrasonic spray (USP) techniques developed in our group.[2,3] Overlayer and catalyst deposition techniques were developed in this project, as described in the Results section. We studied major electrical processes in the photoelectrode and charge transfer from valence band or surface states to electrolyte. We developed corresponding numerical models for several measurement methods (photocurrent, impedance spectroscopy) and calculated responses for typical material parameters. Our optical PEC cell characterization and modeling provides quantitative loss analysis of the device.

Results / findings

The efforts of PECHouse2 led to development of photocathode and photoanode electrodes based on Cu_2O and Fe_2O_3, respectively, as well as exploration of different high-performance materials and various tandem configurations. This section will focus on the results obtained during year three of the project (2014), building upon the results of the first two years, and the results of the previous projects PECHouse and NanoPEC toward the goals of efficient unassisted solar water splitting and the demonstration of a scaled-up device.

Fe_2O_3 photoanodes: overlayers and underlayers [4]

In collaboration with the group of Prof. Juan Bisquert, UJI Spain

Hematite iron oxide (α-Fe_2O_3) was developed into a high-performance photoanode by our group, [2,5] and it remains an interesting and important candidate material for solar water splitting due to its chemical abundance, stability, ease of synthesis, and band gap. However, worldwide progress on hematite has been extremely slow, with few groups reporting photocurrents exceeding 1.0 mA/cm^2 and photocurrent onsets typically occurring at potentials more positive than 1.0 V vs RHE. An ideal

device should have photocurrents exceeding 10 mA/cm^2 and an onset potential of about 0.4 V vs RHE. This means that there are grave challenges in both light absorption and charge separation.

Previous studies in our group (under PECHouse and NanoPEC) established the incorporation of certain underlayers and overlayers toward photoanode performance enhancement,[6–8] but precise understanding of the nature of these enhancements was elusive. We undertook a study of various over- and underlayers by using the electrochemical impedance spectroscopy (EIS) technique with the aim of understanding the surface and interface modifications and their influence on hematite performance, discovering several interesting phenomena.[4] The most interesting findings were that (i) underlayers of Nb_2O_5 and SiO_x can provide doping to thin hematite films, and (ii) Ga_2O_3 overlayer acts to passivate hematite surface states.

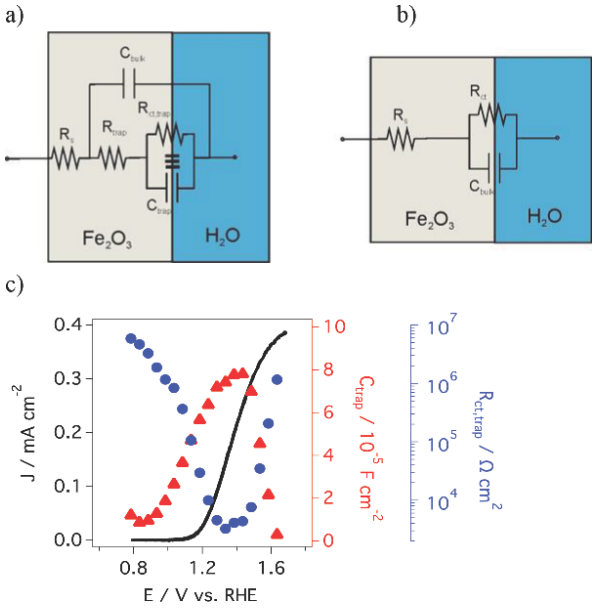

Fig. 1. Physical equivalent circuit model (a) under illumination and (b) in the dark, which was used to extract values of $R_{ct,trap}$ and C_{trap} which correlate strongly with the observed PEC behavior as shown in (c).

In Fig. 1, the equivalent circuit models for the dark and light conditions are shown. By fitting these models to the experimental EIS data, we extracted the potential-dependent behaviors of the resistance to charge transfer from the surface states, $R_{ct.trap}$, and the capacitance of the surface states, C_{trap}. It can be seen that the capacitance increases and the resistance decreases at the potential where photocurrent begins, suggesting that the population of these surface states is a necessary condition for the onset of photoanode current.

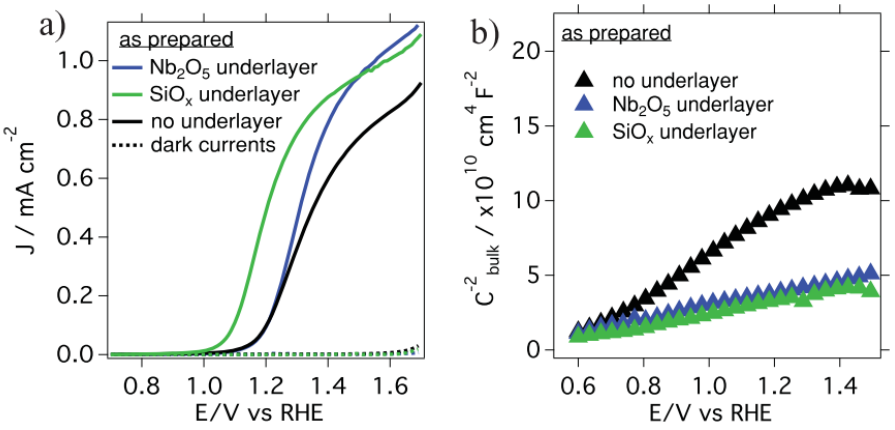

Fig. 2. (a) Current-voltage curves under illumination for hematite with various underlayers. (b) Mott-Schottky measurements for the same samples (in the dark).

For the underlayer treatments, it could be seen that both Nb_2O_5 and SiO_x led to increases in the plateau photocurrent, and this coincides with the measurement of higher dopant densities as seen in the Mott-Schottky plot (Fig. 2). Thus, the higher photocurrents can be explained by a stronger band bending in the surface region of the hematite film, thereby leading to reduced recombination.

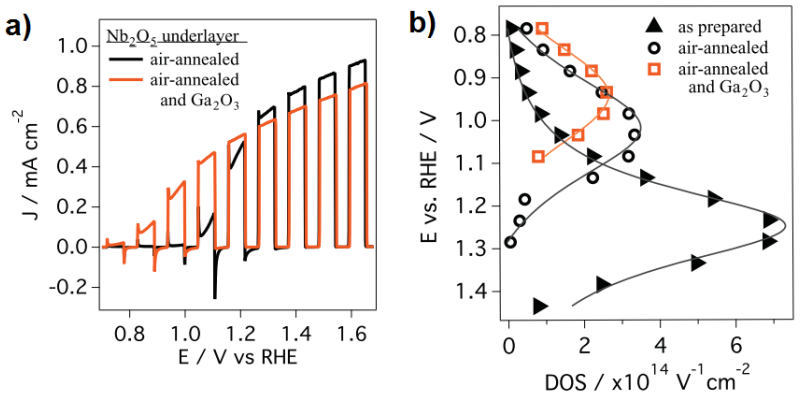

Fig. 3. Hematite device with and without a Ga_2O_3 overlayer. (a) Current-voltage curves showing the onset potential shift, and (b) density of states plot showing the energetic shift of the surface state capacitance.

For samples treated with a Ga_2O_3 overlayer, a large cathodic shift in onset potential, to as low as 0.8 V vs RHE, was attributed to modification of the surface state energetics, as shown in Fig. 3. The density of states was extracted from the measurement of C_{trap} and was observed to both shrink and shift to less positive values upon surface treatment. A more detailed explanation of these findings can be found in the publication.[4] The study demonstrated that EIS can be used to probe the effects of various modifications of a photoelectrode material, and identified two major concepts for improving the performance of thin hematite films, the conductivity as a result of doping and the passivation of surface states. While this study was performed on thin hematite films, the concepts are in principle valid toward higher-performance nanostructured hematite electrodes.

Fe_2O_3 photoanodes: Fe-Ni catalysis and PEC-PV tandem [9]

In collaboration with the group of Prof. Xile Hu, EPFL

For nanostructured hematite, surface and bulk modifications are more difficult due to the complexity and sensitivity of the nanostructure morphology. Our previous efforts used electrodeposited IrO_2 as surface catalyst, yielding record photoanode performances.[2] However, this treatment was not sufficiently stable. Furthermore, catalyst layers of greater transparency were desired. To this end, we developed a new catalyst treatment based on electrodeposition of Fe and Ni to create optically-transparent surface layers on APCVD hematite.[9]

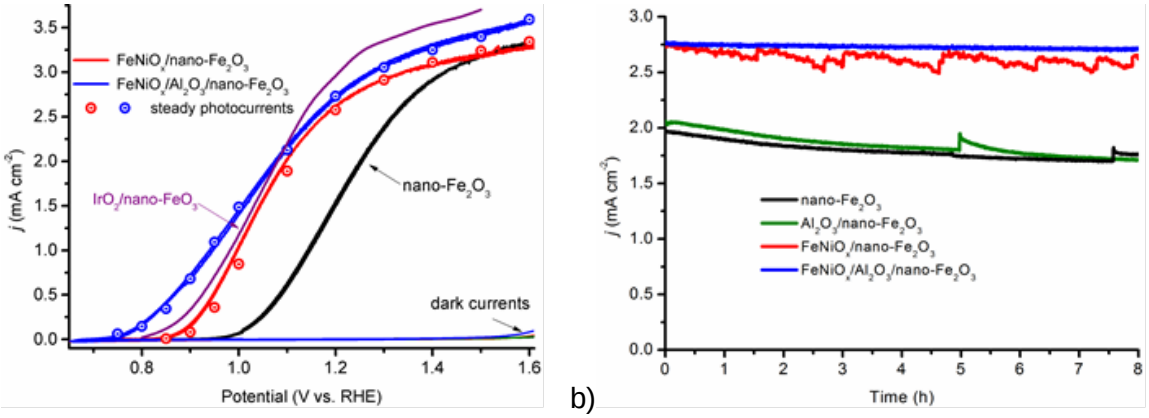

a) b)

Fig. 4. (a) Photocurrent-voltage curves of APCVD hematite with different surface treatments, and (b) photocurrent-time measurements when biased at 1.23 V vs RHE.

The Fe-Ni treatment was based on a simple electrodeposition by repeated linear voltage sweeps in a solution of Fe and Ni salts while illuminating the photoelectrode. Depositing a thin layer of amorphous $FeNiO_x$ totaling only a few nanometers thick resulted in a hematite onset potential of about 0.75 V vs RHE. This provided performances comparable to, or even better than, the record achieved before with IrO_2 (Fig. 4). Importantly, the treatment could yield stable photocurrents over more than 8 hours.

Since this catalyst layer was essentially optically transparent, the overall device transmittance was good and the device could be used as a top component of a stacked multi-absorber system. Our research group has been involved in the recent development of hybrid organic-inorganic perovskites based on $CH_3NH_3PbI_3$ as high-efficiency photovoltaics. Importantly, these devices have been achieving photovoltages of over 1.0 V, and are therefore good candidates for pairing with our photoelectrodes toward achieving overall voltages sufficient for complete water splitting. This Fe-Ni treated hematite electrode was therefore stacked above a perovskite photovoltaic cell, absorbing light of wavelengths up to about 500 nm and transmitting most of the longer wavelengths through to the photovoltaic cell (Fig. 5a).

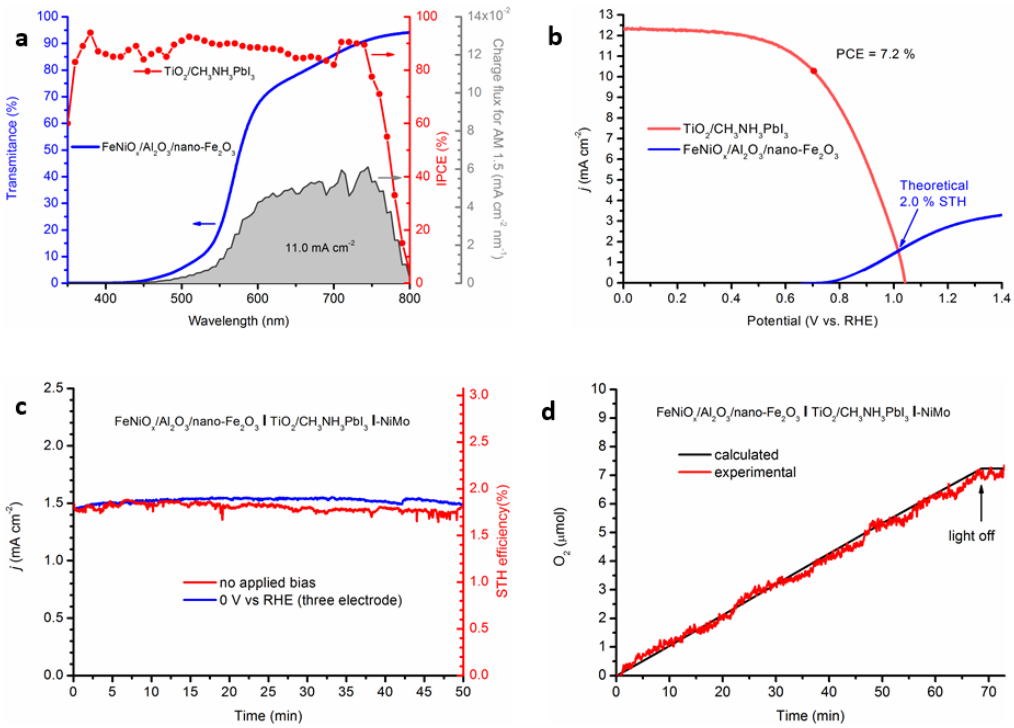

Fig. 5. Hematite/perovskite tandem cell. (a) Light transmittance spectrum of the hematite device compared to the IPCE response of a perovskite photovoltaic cell, combined to predict the photocurrent capability of the perovskite cell when shaded by hematite. (b) Operation point analysis showing the intersection of the photovoltaic cell and photoanode current-voltage curves to predict the operating current of the real and ideal devices. (c) Photocurrent measurement and corresponding solar-to-hydrogen efficiency from a short-circuited device under illumination. (d) Quantification of the evolved O_2 during tandem device operation.

The hematite transmittance is sufficient to provide plenty of light to generate photocurrent in the perovskite. The perovskite cell, when shaded by hematite, gives a short circuit current density of over 12 mA/cm^2 and an open circuit voltage of over 1.0 V. The hematite device, with its photocurrent onset around 0.8 V vs RHE, produces nearly 2 mA/cm^2 at the potential where the two device behaviors cross (Fig. 5b). An ideal hematite electrode with high photocurrent and a steep onset at 0.4 V vs RHE could be capable of over 10 mA/cm^2 in this configuration. The real

unassisted water splitting performance is shown in Fig. 5c, where the tandem device exhibited a stable photocurrent density of about 1.5 mA/cm^2, corresponding to a solar-to-hydrogen efficiency around 1.8%. This efficiency beats that which was previously demonstrated by our group for a PEC-PV tandem using hematite.[10] This study shows that a PEC-PV tandem device can indeed lead to meaningful solar-to-hydrogen conversion, and that the PEC component is still, by far, the limiting component in device performance.

Cu_2O photocathodes: stability enhancement [11]

In collaboration with the group of Prof. Adelio Mendes (Uporto)

The Cu_2O photocathodes developed under the PECHouse and NanoPEC projects represent some of the highest-performing photocathode devices. The TiO_2 protection strategy we developed for Cu_2O [1] has seen widespread implementation by other groups on both photocathodes and photoanodes.[12–14] We recently reported the use of electrodeposited RuO_x as hydrogen evolution catalyst on the protected Cu_2O photocathode,[15] and also MoS_2 in collaboration with Prof. Hu at EPFL.[16]

A crucial feature of any photoelectrode is its stability. Operating under electrochemical conditions can be very corrosive for most materials. While as-deposited ALD layers of amorphous TiO_2 have already been demonstrated by us as rather stable,[15] further improvement is still needed. We have recently published a new hydrothermal (steam) treatment that led to fantastic stability of TiO_2-protected photocathodes.[11] By heating the device in an autoclave containing a small amount of water, to temperatures of only 150 °C, we demonstrated a device capable of stable photogenerated H_2 production over more than 50 hours. As shown in Fig. 6, the steam treatment slightly enhanced the initial device performance and enabled its long-term stability.

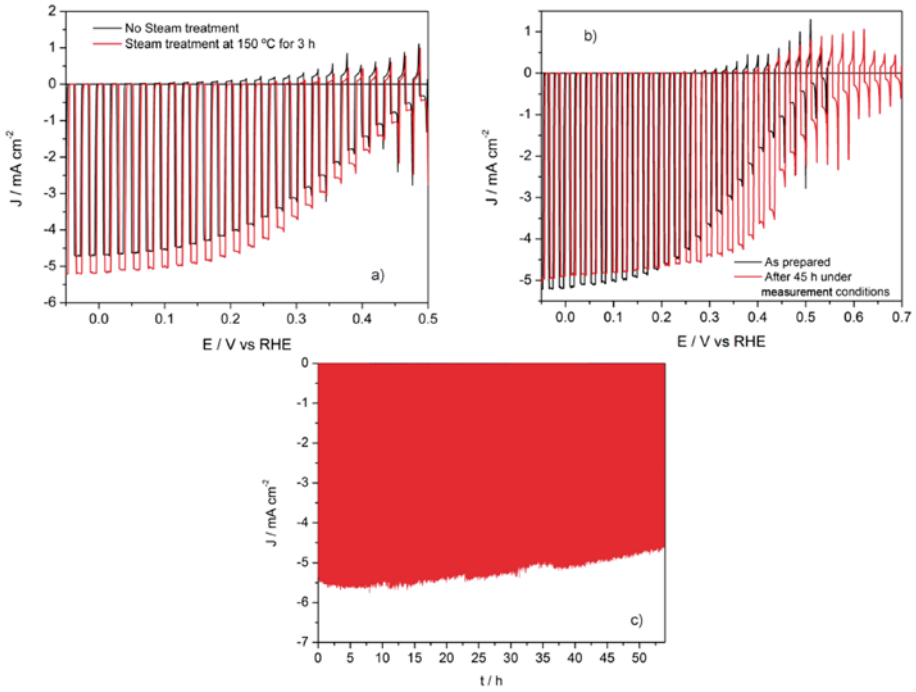

Fig. 6. (a) Current-voltage behavior of the photocathode before and after steam treatment. (b) Behavior of steam-treated device before and after 45 hours of testing. (c) Current under chopped illumination at a bias of 0 V vs RHE.

The effect of the steam treatment was initially mysterious. There were no noticeable changes in the crystallinity of the TiO_2 or its carrier density, but detailed microscopy pointed to an overall smoothing of the film morphology. It is likely that the steam treatment helped make the overlayer more uniform and continuous, reducing the prevalence of small “pinholes” which may allow the solution to contact the Cu_2O or AZO materials and thereby corroding them. This treatment pointed to a promising

avenue of enhancing stability of devices employing protective overlayers.

Cu_2O photocathode: transparent Cu_2O and tandem with perovskite [17]

In collaboration with the group of Prof. Adelio Mendes (Uporto)

For a tandem configuration, the Cu_2O photocathode should be paired with a smaller-bandgap device capable of utilizing the lower energy photons of the solar spectrum. In a stacked configuration, the photocathode would therefore need to be optically transparent to these photons. Our typical synthesis of Cu_2O involves cathodic electrodeposition onto Au-coated FTO/glass substrates, which offer no transparency. We found that bare FTO, however, yielded low-quality deposition of Cu_2O and poor device performance that was likely due to an unfavorable electronic junction between FTO and Cu_2O. Therefore, the gold is necessary but renders the device opaque. We recently discovered a method of drastically reducing the amount of gold used while simultaneously enabling highly-transparent photocathodes.[17]

Rather than sputtering Au films of 150 nm, we employed a brief sputter deposition of a 3 nm equivalent. This did not yield a continuous film but rather scattered “droplets” of Au across the textured FTO surface. Nonetheless, this Au-treated substrate enabled dense Cu_2O electrodeposition, as shown in Fig. 7.

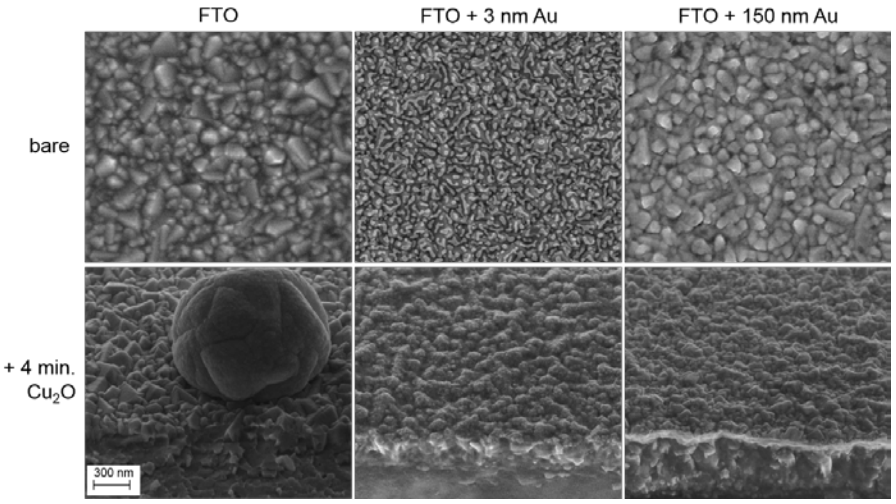

Fig. 7. SEM images of FTO/glass substrate before (top row) and after (bottom row) 4 minutes of Cu_2O electrodeposition. The columns are labeled with the substrate condition.

Although the Au was not continuous over the substrate surface, the device performance was nearly as good as the typical device based on thick Au. As shown in Fig. 8a, Au free devices had poor photocurrent while 3 nm of Au enabled good performance. Fig. 8b shows that the device transmittance begins around 500 nm and reaches around 30% for the red region of the spectrum.

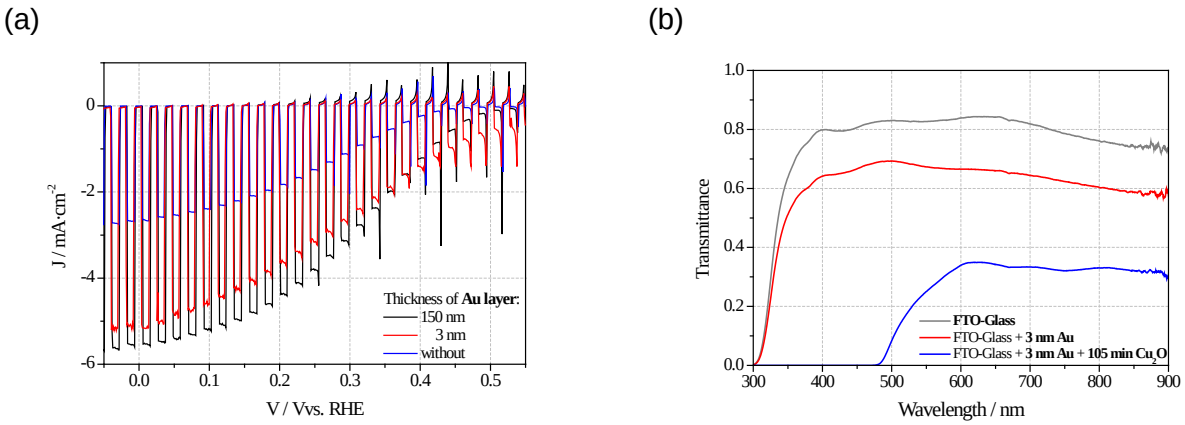

Fig. 8. (a) Current-voltage curves for photocathodes on substrates of various substrates. (b) Transmittance spectra of substrates and device.

The transmittance of this device allows it to be coupled above a smaller bandgap device for tandem operation. We chose to employ a perovskite photovoltaic cell to assemble a PEC-PV tandem. In Fig. 9, the performances of the individual components and complete tandem are shown. It has been concluded that a real-world water splitting device must operate under extreme pH, either acidic or alkaline, in order to prevent the accumulation of a pH gradient which would stop the device from functioning. We therefore tested the Cu_2O photocathode (with AZO/TiO_2 overlayers and RuO_x catalyst) in 1 M NaOH, and we found it to perform very well, even better than in the pH 5 solution previously employed. The demonstration of a photocathode in alkaline solution is important since in a complete device there must also be an anode carrying out water oxidation, and most water oxidation catalysts function best in alkaline solution.

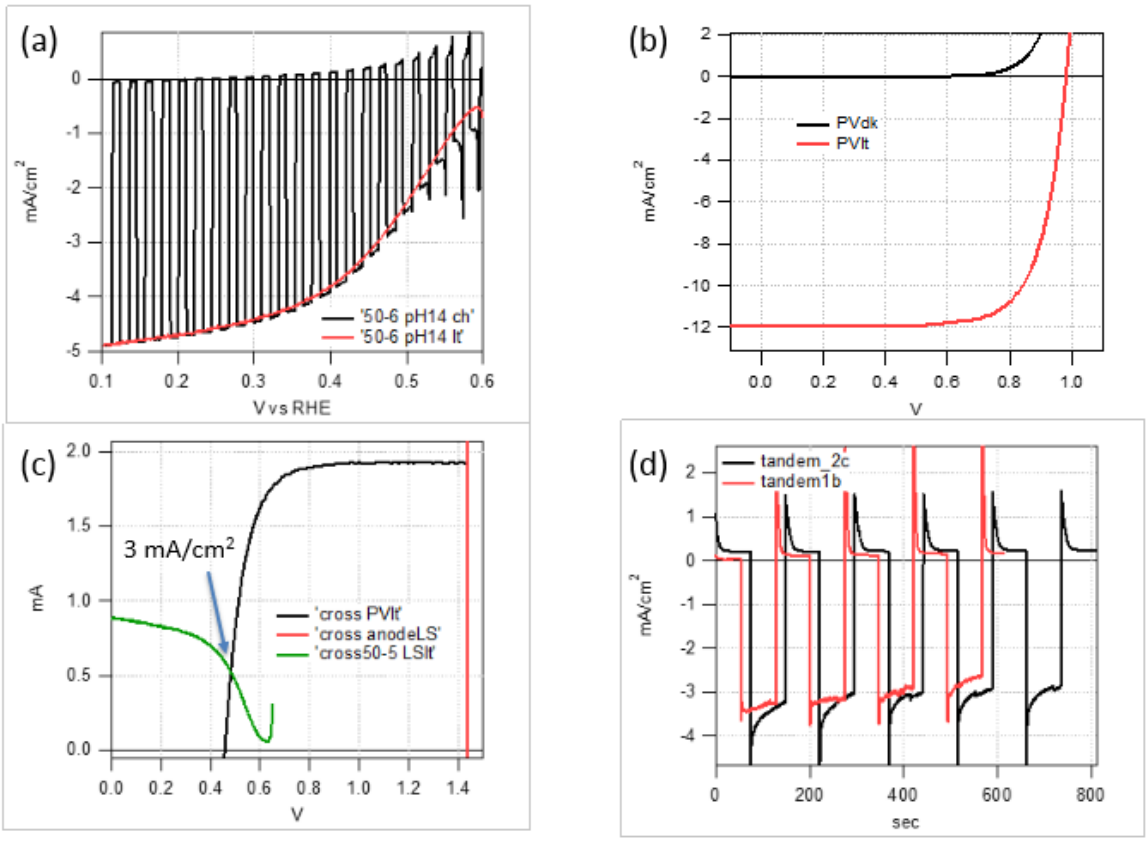

Fig. 9. PEC-PV tandem performance. (a) Current-voltage performance of Cu_2O

photocathode in 1 M NaOH solution. (b) Current-voltage curve of the perovskite photovoltaic cell behind the transparent Cu_2O photocathode. (c) Combination of photocathode, photovoltaic cell, and anode curves to determine the predicted operation point. (d) Short circuit current under chopped illumination, showing around 3 mA/cm^2 of unassisted water splitting.

The perovskite photovoltaic cell produced an open circuit voltage of about 1 V, and combining the photovoltaic, photocathode, and a Ni-Fe anode gave the operation point prediction shown in Fig. 9c. This current density of 3 mA/cm^2 was confirmed in the short circuited device, a performance that corresponds to about 3.7% solar-to-hydrogen conversion efficiency. The photocurrent slowly decayed over the course of two hours to less than 1 mA/cm^2, a result of the corrosive NaOH degrading the device through defects in the TiO_2. Since TiO_2 should be stable under these conditions, further attempts to stabilize the TiO_2 must be coupled to the continued testing of the photocathode in alkaline solution, including the steam treatment described above.

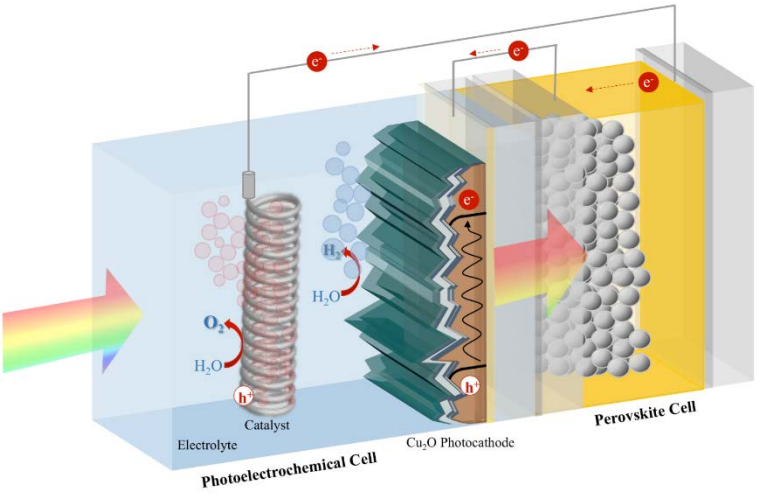

In collaboration with Prof. Hu, we have also found that the Cu_2O device using earth-abundant catalysts MoS_2 or Ni-Mo can function well in strongly alkaline solution, a result that was recently published.[18] However, our RuO_2 catalyst treatment still outperforms those devices in terms of photovoltage, a result that will soon be published.[17] The present result represents one of the best performing PEC-PV tandems to date, enabled by our development of the Cu_2O photocathode over the course of the PECHouse projects and the development of the perovskite photovoltaic technology in our group.

Deliverable 1.21: Large-scale tandem

The final deliverable of PECHouse2 was to develop a photoelectrode device with solar-to-hydrogen conversion at very high efficiency, and demonstration in a large-scale format with extreme stability. We have made good progress on each component individually (photoelectrode performance, electrocatalysts, stability enhancement, etc.), but it is a great challenge to combine all that knowledge onto a larger scale device. Indeed, achieving the performance benchmarks of this deliverable would represent an incredible breakthrough in the field of PEC-based solar-to-H_2 research. It is estimated that the threshold for commercial viability entails efficiencies of around 10%,[19] so the goal of scaled-up devices exceeding efficiencies of 10% represent an important benchmark toward commercialization.

We focused the large-scale tandem efforts on our high-performance Cu_2O photocathode as it promises to give the best tandem performance and to be most readily scalable among the devices we've studied. The tandem concept of choice is to couple the photoelectrode to a photovoltaic cell, which are simultaneously illuminated by different regions of the spectrum to generate photocurrent and photovoltages that combine to exceed what is necessary for water electrolysis.

The first consideration was to establish the PEC-PV configuration for the best chance of success. While we have good preliminary results on transparent Cu_2O (above),[17] using a thick Au substrate still gives the best performance, and the approach of using a dichroic mirror to split the spectrum offers more control and flexibility than a stacked tandem. Therefore we chose to use top-down illumination onto a 45° angled dichroic mirror with a cut-off at 675 nm, as depicted in Fig. 10. This "cold mirror" allows the direct transmission of the red and IR region (>675 nm) while reflecting sideways the higher-energy visible photons (<675 nm). As shown below, this allows large-area illumination of our photocathode in vertical configuration with illumination of a photovoltaic module below the mirror. The large photovoltaic we employed was a monocrystalline silicon module prepared by our collaborators in the group of Prof. Ballif (EPFL PV-LAB).

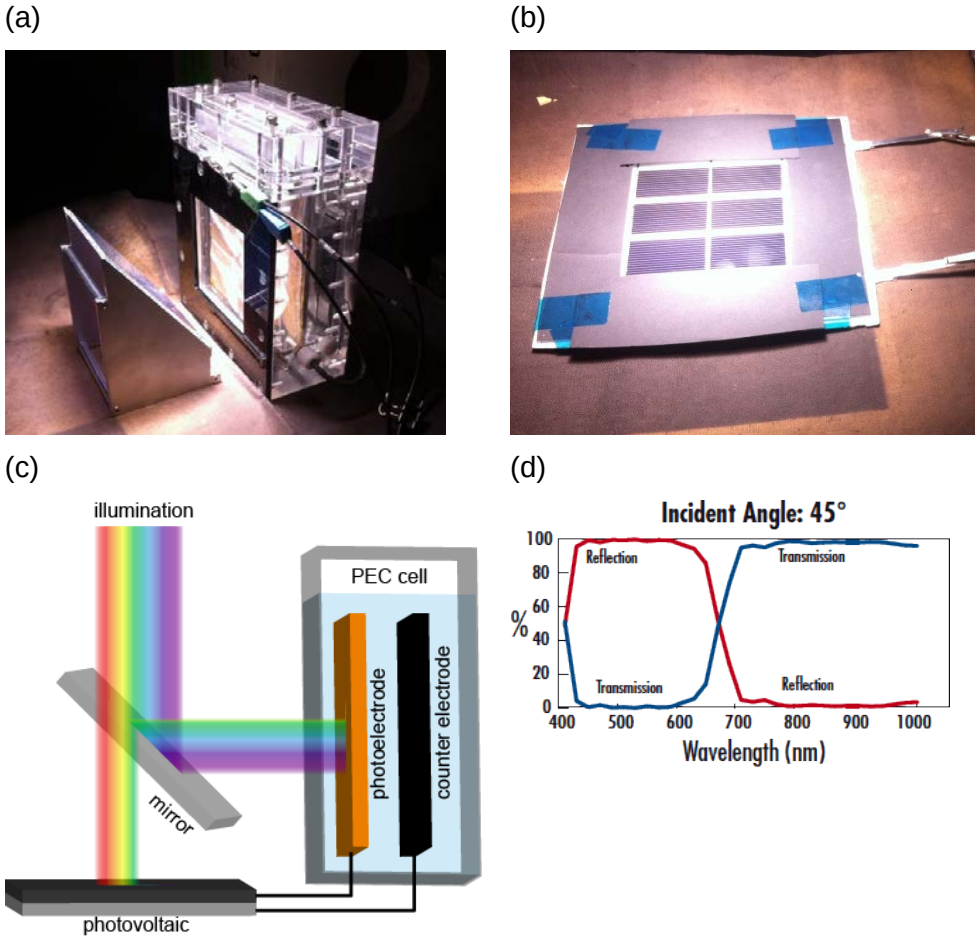

Fig. 10. PEC-PV tandem configuration employing a dichroic mirror. (a) PEC cell and mirror, (b) Si module, (c) spectrum splitting schematic, (d) mirror characteristics (Edmund Optics).

The second task was to develop a photocathode fabrication processes compatible with the targeted large scale area. Since we are limited by the size of our ALD apparatus, the 100 cm^2 device was assembled as a 2x2 module of 25 cm^2 devices. The Cu_2O electrodeposition and overlayer ALD deposition processes work well on these scales, although possible non-uniformity in the ALD overlayer thicknesses can lead to device performance anomalies. The catalyst deposition based on photo-electrodeposition of RuO_2 also works reasonably well on the 25 cm^2 devices. The four components were fixed together and put into a large PEC cell designed by our partners from NanoPEC (A. Mendes, UPorto).

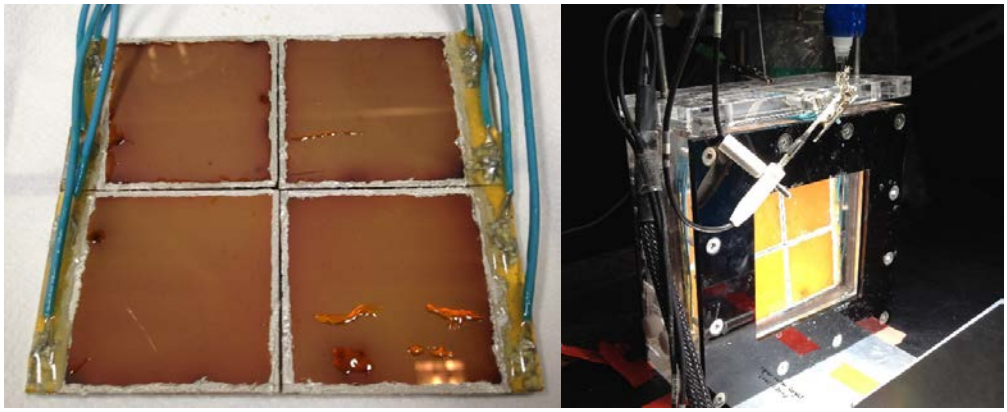

Fig. 11. Photographs of the 2x2 mosaic device totaling 100 cm^2 active area.

A large area top-down solar simulator was used to shine down onto the mirror, illuminating the Si module and the PEC cell. A 3-electrode measurement of the photocathode itself showed a reasonable performance (Fig. 12a), with an onset around 0.5 V vs RHE and a photocurrent reaching -5 mA/cm^2, both being typical values observed on small-scale devices (<1 cm^2). This promising observation confirmed the scalability of our synthesis methods, but the poor fill factor of the J-V curve suggests the catalyst deposition was not optimal. Efforts are underway to improve methods of large-area catalyst treatment.

The choice of photovoltaic technology was based on the spectral utilization (must be sensitive to photons of wavelength >600 nm not used by Cu_2O) and the voltage requirement for tandem operation. The best choice for a large scale module was monocrystalline silicon, which we obtained from our collaborators in the Ballif group. Based on the PEC response of the photocathode, and the knowledge that the anode counter electrode would require an overpotential beyond the 1.23 V vs RHE that defines the oxygen evolution reaction, we needed a solar cell that could provide more than 1 V. A Voc of greater than 1.5 V would be more ideal, as it should provide enough voltage to operate the photocathode near its plateau photocurrent (about 5 mA/cm^2 as shown in Fig. 12a). This was accomplished by using a triple Si module, series connected to produce a Voc of about 1.7 V (Fig. 12b).

To predict the operation of the tandem, the significant anode overpotential must be accounted for, which is why the PV J-V curve is shifted to start at about 1.6 V vs RHE in Fig. 12c. The photovoltaic cell was measured behind the dichroic mirror, and the Cu_2O used the reflected light from the mirror. The crossover point of the PEC and PV cell components occurred at a photocurrent around 4.2 mA/cm^2, which would correspond to a solar-to-hydrogen efficiency of about 5.2%.

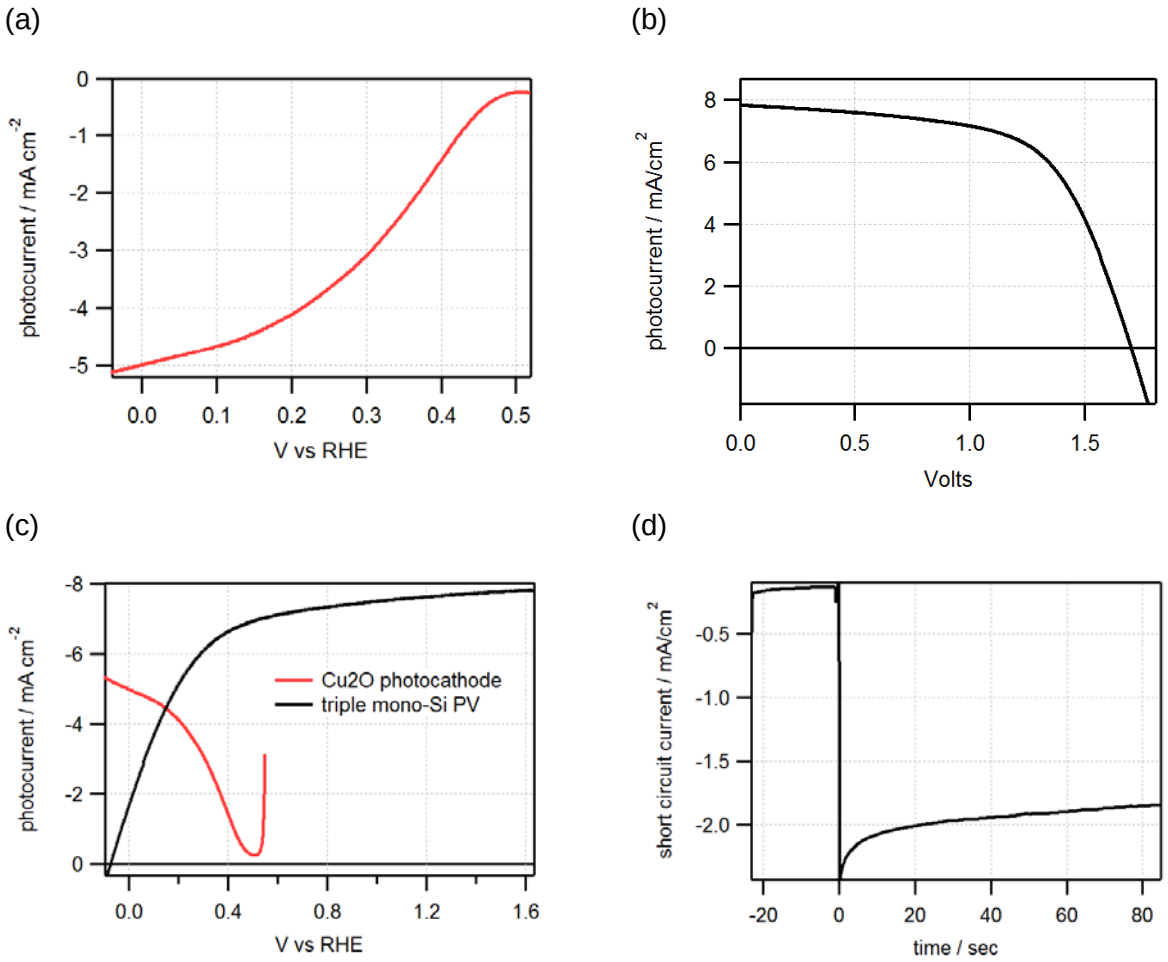

Fig. 12. Current-voltage curves after spectrum splitting for (a) the large photocathode, (b) the Si photovoltaic, and (c) both overlaid for operation point analysis, and (d) short-circuit, unbiased water splitting current in dark then under 1 sun illumination.

When electronically connecting the PV cell, photocathode, and anode in short circuit, the actual unassisted water splitting current was observed. As shown in Fig. 12d, the photocurrent was considerably smaller than the predicted point. It began at around -2 mA/cm^2 then gradually decreased.

The first culprit to the lower observed currents is the fact that the complete device, when short circuited, has significant overpotentials that do not appear in a 3-electrode system. In the pH 5 electrolyte used here, the conductivity by ion transport is much poorer than in acidic or alkaline solutions, leading to a potential drop due to the solution resistance. Furthermore, continued operation of an electrolysis system in near-neutral conditions leads to a pH gradient build-up, adding an overpotential which counteracts the device photopotential. For these reasons, electrolyzers, and future PEC-PV tandem designs, need to operate in acidic or alkaline solutions.

The device performance would therefore be expected to be better in 1 M NaOH, as explored in the previous section. It is known that the Cu_2O photocathodes are not yet very stable in alkaline solution, however, so this remains a crucial point for future study. The 2 mA/cm^2 reported here, while short of the 7 mA/cm^2 target for 10% STH efficiency, represents an important step in complete sunlight-driven water splitting systems, especially given the fact that it was accomplished on a 100 cm^2 scaled device. With better cell design and enabling the Cu_2O photocathode in alkaline solution, 6 mA/cm^2 should be achievable from this system. To move beyond that photocurrent, materials with higher quantum efficiency are needed, either by modifying Cu_2O, or by looking to other existing materials, as discussed next. As described below, photocathodes based on CIGS are expected to achieve 10% STH in a PEC-PV tandem configuration.

The demonstration of a 100 cm^2 device showed that the principles developed on small-scale prototypes (> 0.5 cm^2 typically) can be preserved on a larger, more realistic scale. Notably, in three-electrode tests the large photocathode performance, as shown in Fig. 12a, was equivalent to that of small devices, with an onset potential around 0.5 V vs RHE and a photocurrent density reaching 5 mA/cm^2 despite the much larger area. This shows that scale-up of this device configuration is realistic and achievable. The stability goal of 1000 hours (extrapolated) with less than 10% degradation remains a challenging goal. Much progress has been made on the stability of TiO_2 protected photocathodes, as described previously,[11] but more work is necessary to translate these enhancements onto the large-scale device. Significant progress was made toward each goal (scale, stability, and performance) and new developments described below point to further advances in the near future.

CIGS photocathode: a new high-performance photocathode

In collaboration with the group of Prof. Tiwari (EPMA)

While our group has made great progress on metal oxides for PEC water splitting, it is important that we keep an open mind to other materials. Namely, the development of $CuIn_xGa_{1-x}Se_2$ in photovoltaics demanded that we consider it for PEC applications. This p-type absorber material has a bandgap that is tunable between 1.0 and 1.7 eV (based on the In:Ga content), which being smaller than Cu_2O offers the chance at higher photocurrents. The typical CIGS/CdS/ZnO junction shares some similarity with the Cu_2O/AZO/TiO_2 junction employed in our photocathodes. We therefore sought to adapt our photocathode device to feature CIGS as an absorber material, applying the AZO/TiO_2 overlayers by ALD on top of the CdS-treated CIGS surface. The CIGS/CdS samples were provided by a new collaboration with the group of Prof. Tiwari (EMPA).

(a)

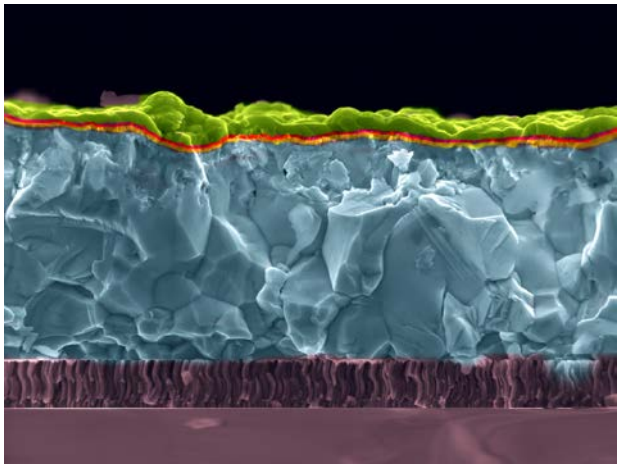

(b)

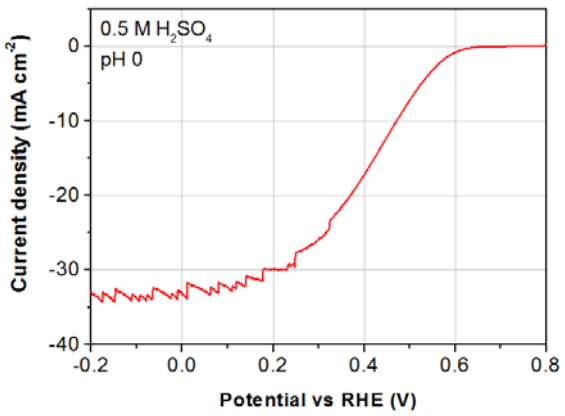

(c)

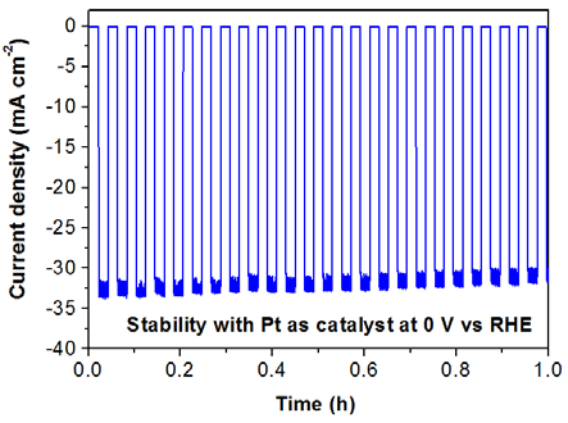

Fig. 13. (a) SEM cross section of CIGS device. (b) J-V curve in pH 0 with Pt catalyst. (c) Current under chopped illumination when biased at 0 V vs RHE.

We immediately realized a fantastic PEC response from this device (upon treating with catalyst Pt or RuO_2) (Fig. 13). First, the onset potential occurred at about +0.6 V vs RHE, comparable to the best onsets previously seen on Cu_2O devices. This is despite the fact that the band gap, and thus the theoretical photovoltage, is smaller for CIGS than for Cu_2O, and points to the quality of the p-n junction in the device. Secondly, the photocurrent plateau is very high, exceeding -30 mA/cm^2 at 0 V vs RHE. This results from the smaller bandgap, which allows a broader spectral utilization, and the material furthermore exhibits a high quantum efficiency across the spectrum.

This preliminary result points to a clear path of future study. The high performance in terms of photovoltage and photocurrent suggests the possibility of implementing CIGS in high performance tandem configurations. The goal of 10% solar-to-hydrogen requires 7 mA/cm^2 of unbiased water splitting photocurrent. These findings with CIGS photocathodes reveal a path toward accomplishing this goal. The CIGS photocathode reaches remarkable currents of over 33 mA/cm^2 under one-sun illumination, and can therefore accommodate the reduction in its photocurrent when incorporated into a spectral splitting tandem. A tandem between a CIGS photocathode and a photovoltaic (Si or perovskite) is predicted to reach the goal of 10% STH, and a scaled up demonstration of this system is presently under construction.

Perovskite-driven electrolysis with high efficiency [20]

In the PEC-PV tandem described above, we employed an external photovoltaic module to supply the additional photovoltage toward complete water splitting. With the new developments in perovskite PVs, a single cell can achieve photovoltages of 1.0 V or greater, which is better than the 0.6-0.7 V of conventional silicon solar cells and is competitive with solar cells made from expensive processes and materials. This makes perovskites a good candidate for PEC-PV tandem, as reported in a previous section.

With electrolysis requiring typically at least 1.8 V to run efficiently, we realized that these 1 V perovskite cells enabled a new achievement in PV-driven water splitting. By simply connecting two of them in series, a module could achieve a Voc of 2.0 and a Jsc over 10 mA/cm^2. In parallel we were developing new electrocatalysts for water splitting, namely a hydrothermal synthesis of Ni-Fe layered hydroxides on Ni foam substrates, which we discovered to be bifunctional for use as both anode and cathode. These electrodes were capable of supporting 10 mA/cm^2 at a 2-electrode voltage of just 1.5 V. As shown in Fig. 14c, driving these electrodes with a double perovskite cell would be predicted to give 12.3 solar-to-hydrogen conversion efficiency. We assembled the full device and indeed achieved this efficiency, as shown in Fig. 14d.[20]

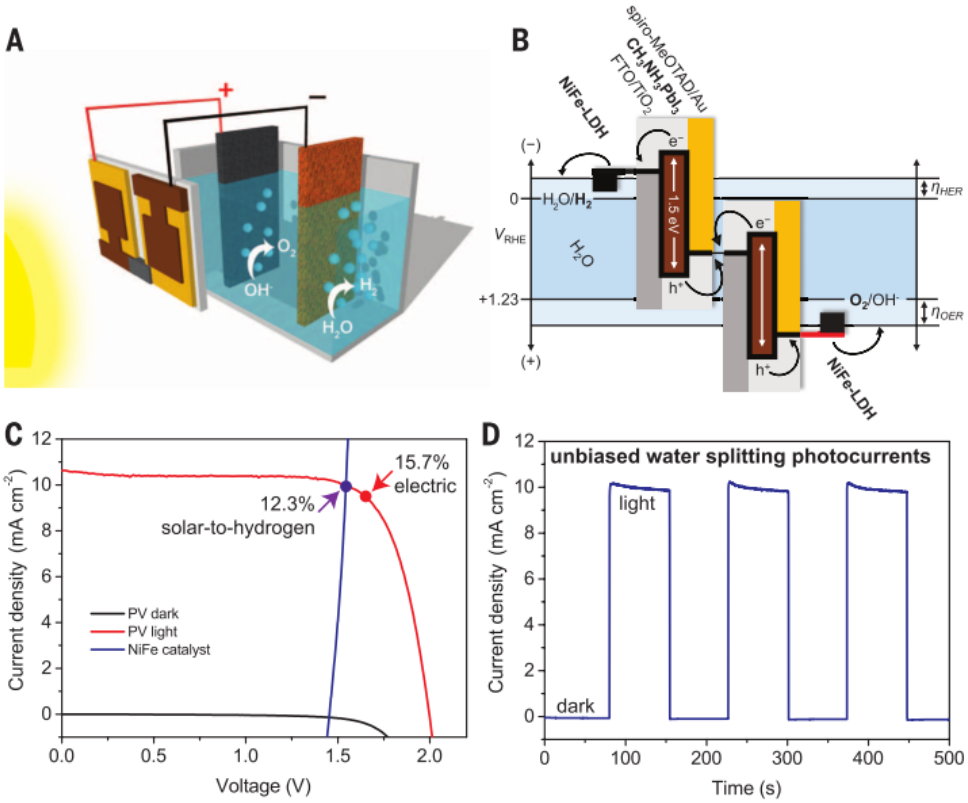

Fig. 14. (a) Device schematic, (b) energy diagram, (c) operation point prediction, and (d) unbiased water splitting currents under chopped 1 sun illumination.

This result was published in the journal Science and received a lot of attention. This is because it demonstrated a record STH efficiency for devices based on earth-abundant materials and low-temperature solution-based synthetic processes. Turner et al. had achieved similar performance a decade ago but using an expensive GaAs/$InGaP_2$ device.[21] Recently, Nocera et al. performed a very similar demonstration to what we showed, but using instead as many as four series-connected Si cells to achieve 10% STH.[22] Meanwhile, the JCAP project has yet to publish a device which achieves unassisted water splitting.

This device achieved high efficiency even despite the fact that the two perovskite cells were identical, using the same region of the solar spectrum, and were side-by-side, thereby doubling the active area (and thus halving the current density). Further improvement would be to use a perovskite cell in an optical tandem configuration, coupled with candidate materials such as CIGS or silicon. An ideal tandem between state-of-the-art perovskite and a Si HIT cell could be expected to achieve STH efficiencies exceeding 16%. Such approaches are already predicted to achieve 30% photovoltaic efficiency,[23] and these efforts are presently underway in our group.

Deliverable 1.15: Loss Analysis

"Account of loss analysis of a solar water splitting device."

The optical losses in a photoelectrochemical (PEC) cell account for substantial part of the solar-to-hydrogen conversion losses, but their quantitative analysis is sparse partially because the optical losses cannot be measured directly in the experiment and their quantification requires accurate knowledge of optical constants of all individual layers. In course of the PECHouse2 project, ZHAW and EPFL worked together to present a detailed analysis of the optical losses of typical PEC cell based on the combination of spectroscopic measurements and an optical model of both coherent and incoherent layers. We determined wavelength-dependent reflection, transmission and absorption outside of the semiconductor, maximum incident photon-to-current efficiency and charge

generation rate. The optical model has been verified for hematite by atomic layer deposition (ALD). A detailed description of our work is available in manuscript of Ref. 26 in the Appendix A.

In a typical PEC cell configuration as shown in Figure 11 light is interacting with multiple layers of different optical properties. Each of the layers needs to be included during optical modeling with accurate complex index of refraction. Our model describes light propagation in coherent layers (thickness comparable to wavelength of light) with the transfer-matrix method and in incoherent layers (thickness larger than wavelength of light) by ray-tracing geometrical optics. Energy conservation is fulfilled throughout the simulation.

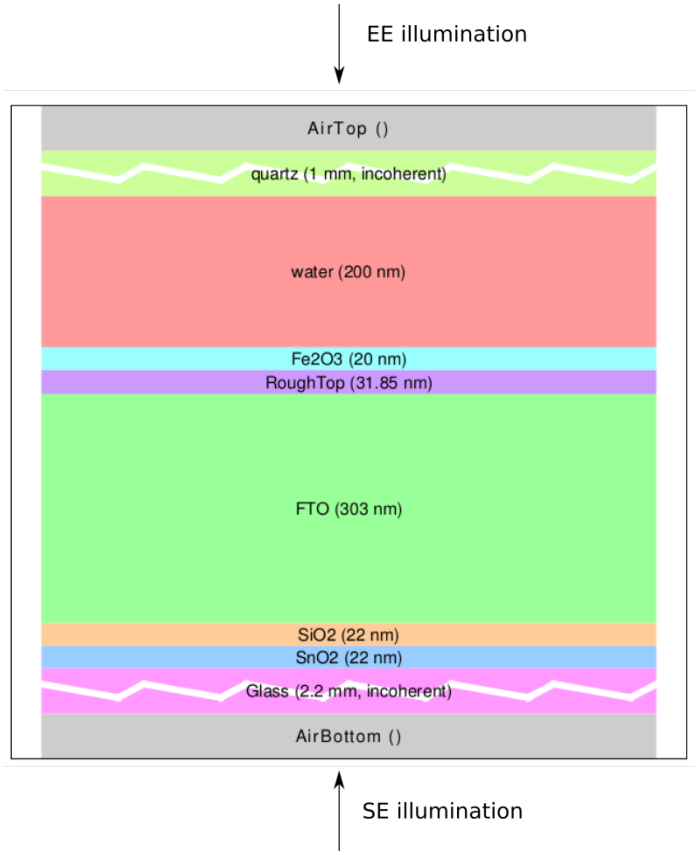

Fig. 11. Sketch of the PEC cell layer sequence used for UV-Vis measurements and simulations. Thicknesses of the layers are scaled for the purpose of presentation.

First, the optical constants of the individual layers of the photoelectrode (Q, H, F, Si, Sn, G) were determined by combination of literature values and parameter extraction from spectroscopic ellipsometry and UV-Vis spectroscopy (Ref. 26 and Supporting Information in the Appendix) and then implemented them in our optical model. Extracted optical constants of hematite are shown on Fig. 12. The extinction coefficient for our ALD hematite is larger than reported by Martinson et al. pointing to the film deposition differences even between two different ALD fabrication setups. The refractive index our ALD hematite varies around ≈3, which implies large optical reflection losses due to the large optical contrast on the water-hematite interface (quantified later in Fig.14).

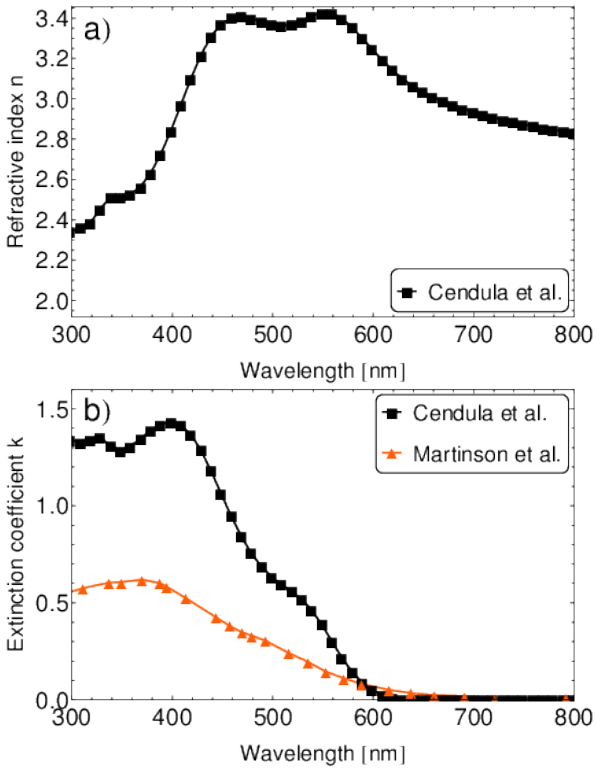

Fig. 12. Optical constant of hematite extracted from ellipsometry of two layers HQ, a) refractive index and b) extinction coefficient.

The proper parametrization of the optical constants is confirmed with the ability of the optical model to reproduce UV-Vis measurements on various test cells, Fig. 13. We assembled multilayers QWHTiQ (Quartz,Water,Hematite,TiO_2,Quartz) and QWHTiT (Quartz,Water,Hematite,TiO_2,TEC15) in order to confirm predictive abilities of our optical model and we obtained good overlap of the reflectance and transmittance measurements and simulations for electrolyte-electrode (EE) illumination, Figure 3 (comparison for substrate-electrode illumination SE is also available in Supporting Information). The transmittance of QWHTiQ is ≈0.4 for 300 nm < λ < 400 nm wavelengths and increases then to ≈0.9 at λ =700 nm as a consequence of less light absorption in hematite in this wavelength range. The reflectance of QWHTiQ is ≈0.2 for 300 nm < λ < 600 nm and then decreases to ≈0.1 at λ =800 nm due to the large mismatch of refractive index of water/hematite interface (≈ 1.35/3). The transmittance of QWHTiT and

QWHTiQ show similar profile and the QWHTiT reflectance for 300 nm < λ < 400 nm reproduces correct valley and peak positions and magnitude of the measured specular R_{spec} reflectance. The total reflectance consists of the specular and diffusive reflectance $R_{tot} = R_{spec} + R_{diff}$. Decrease in reflectance losses from ≈0.2 to ≈0.04 could be achieved by using anti-reflective coatings on the surface of the cell.

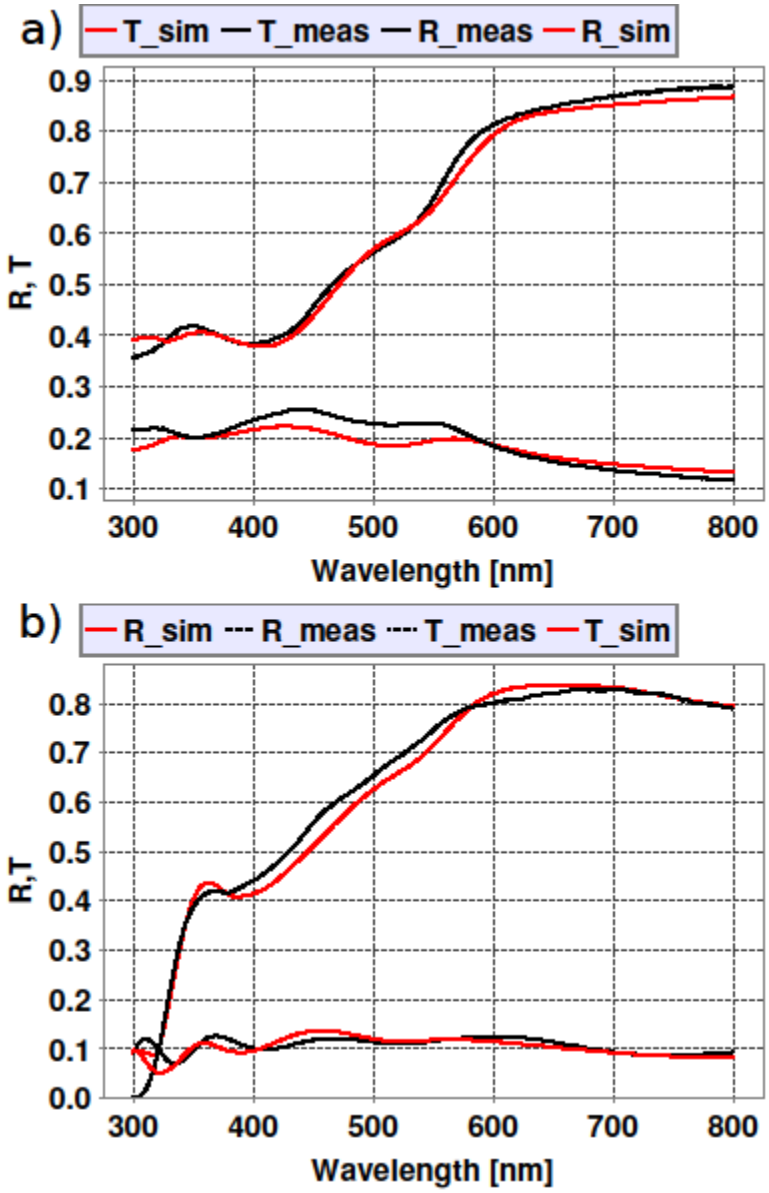

Fig. 13. Comparison of measured (black) and fitted (red) reflectance and transmittance of 12 nm ALD hematite, EE illumination for a) QWHTiQ and b) QWHTiT..

We used our validated optical model to calculate spectrally resolved optical losses in the PEC cell and to obtain the total integrated optical losses by reflection, transmission and absorption in the PEC cell at LPI EPFL. The thickness of ALD hematite is 12 nm and the thickness (width) of the electrolyte in this cell is 0.4 cm. Valuable insights into the optical losses in the individual layers are presented in Figure 14. The calculated reflectance R_{tot}, absorptances in the individual layers A_l and transmittance T_{tot} for EE and SE illumination are shown in a stacked diagram and satisfy the energy conservation. The fraction of the reflected, transmitted and absorbed light in the individual layers is spectrally dependent. This fraction also strongly depends on the illumination direction.

For EE illumination, Figure 4a, the absorptance in hematite is ≈0.4-0.5 for 300 nm < λ < 400 nm, afterwards decreasing to zero near λ =600 nm (corresponding to wavelength of its bandgap energy). Nearly constant absorption loss of ≈0.1 can be seen for SnO_2 :F over whole wavelength range and glass absorption is largest for λ < 350 nm (up to ≈0.2) and for λ > 600 nm (which is uncritical given the cease of hematite absorption for λ > 600 nm). The absorption in water and

quartz is negligible in the presented data. For SE illumination, Figure 4b, the absorptance in hematite for λ <400 nm is smaller compared to EE illumination due to much stronger absorption in float glass which stands in the SE light path before hematite. The absorption in SnO_2 :F for SE illumination is slightly larger than for EE illumination. Reflectance for both EE and SE illumination makes ≈0.1-0.2 but the interference fringes of SnO_2 :F are more pronounced for the SE illumination. Decrease in reflectance losses from ≈0.2 to ≈0.04 could be achieved by using anti-reflective coatings with established techniques. Table 1 shows the integrated losses in terms of photocurrents eq. 3 corresponding to different physical processes in the PEC cell. The sum of these respective channels gives the maximum possible photocurrent for hematite ≈12.5 mA/cm2.

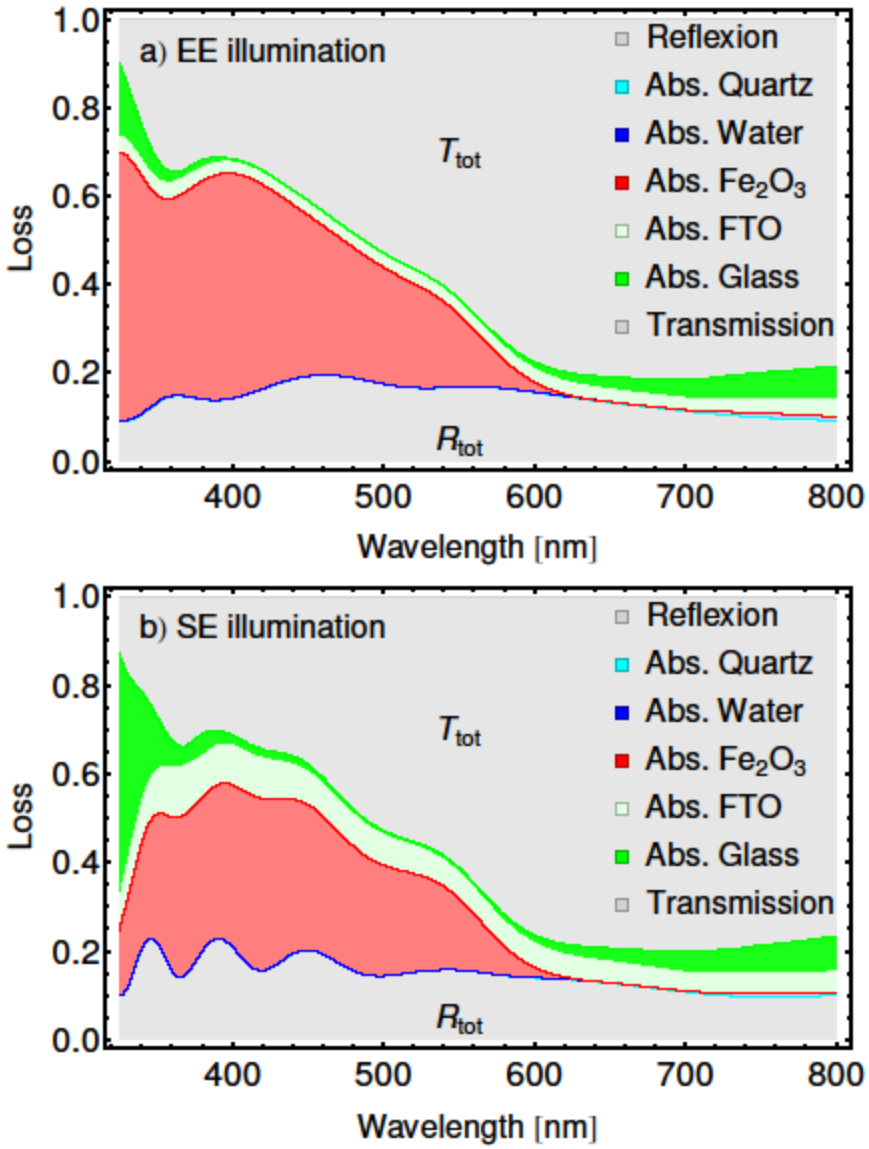

Fig. 14. Detailed optical loss analysis of a PEC cell with a) EE and b) SE illumination. The calculated total reflectance, the absorptance in each layer and the total transmittance are stacked and colored in the graphs.

Optical loss	EE [mA/cm^2]	EE [%]	SE [mA/cm^2]	SE [%]
Reflection	2.1	17	2.0	16
Abs. Quartz	0	0	0	0
Abs. Water	0	0	0	0
Abs. Hematite	3.5	28	3.0	24
Abs. SnO_2:F	0.3	3	0.9	7
Abs. Glass	0.1	1	0.3	3
Transmission	6.4	51	6.2	50

Table. 1. Optical loss channels for 12 nm ALD hematite in terms of photocurrent.

The absorptance in the hematite layer A_{Fe2O3} is in close relation to the incident photon-to-current efficiency (IPCE) which gives the ratio of the number of electrons in an external circuit divided by the number of incident photons on the device. If we assume that every absorbed photon in hematite layer contributes electron in the external circuit (absorbed photon-to-current efficiency APCE = 1) then the absorptance in the hematite is equal to the maximum theoretically achievable IPCE according to $IPCE_{max} = A_{Fe2O3}$. $IPCE_{max}$ from our optical simulations is larger than our measured IPCE data at 1.43 V vs. RHE due to the inefficient collection of photogenerated charges (most of them recombine before contributing to photocurrent), Figure 15. The values of $IPCE_{max}$ represent an upper limit of the achievable IPCE in ideally collecting hematite photoelectrode which is readily not the case for our photoelectrode. For increasing thickness of hematite 8, 12, 16 nm, the IPCEmax increases only slightly. However, keeping in mind the hole diffusion length of 2-4 nm reported for hematite, thicknesses larger than 4 nm suffer from inefficient charge transport, thereby, decreasing the photoelectrochemical performance.

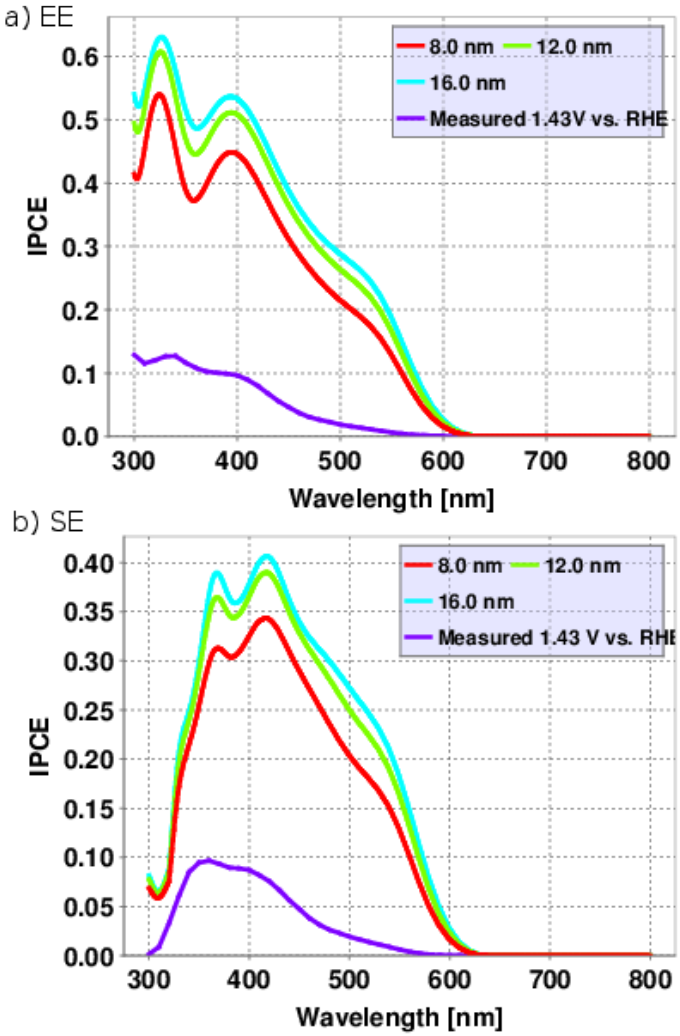

Fig. 15. Calculated $IPCE_{max}$ of hematite films for thicknesses 8 nm, 12 nm, 16 nm and our measured IPCE data at 1.43 V vs. RHE. a) EE and b) SE illumination..

The optical model is also used to calculate a charge generation profile which is used as direct input for electrical model of the photoelectrode and thus enable coupled optoelectronic modeling of the photoelectrode. The wavelength-dependent quantification of optical losses in PEC cells and its software implementation allows for detailed optimization of optical absorption and electrical collection in dual-absorber PEC cells and systems.

Deliverable 1.14: Modeling Report

Part of this work was an internship and bachelor thesis of Maria Jarolin (TU Berlin) in collaboration with R. van de Krol (Helmholtz Zentrum Berlin)

The aim of this section was to develop a numerical model of the impedance measurements and to extract physical parameters of the hematite photoelectrode from their comparison with simulations. A frequent approach in the recent literature (and also used above by LPI EPFL during investigations of over- and underlayers in Fe_2O_3) is to use equivalent circuits consisting of a combination of charge transfer resistances and capacitances. Lumped values of these resistances and capacitances are then extracted from a comparison of impedance calculations and measurements. Although such

values allow for a phenomenological comparison of different samples, the equivalent circuit approach is ambiguous in nature: it does not provide access to values of basic physical and photoelectrochemical properties (that is, rate constants for processes) of hematite. Therefore, in our previous Deliverable D 1.12 we presented a basic physical model of charge transfer with surface states on the semiconductor-electrolyte interface (zero-dimensional model) and discussed the need for its extension to account for a drift-diffusion model in the semiconductor bulk (one-dimensional model). This approach includes surface states kinetics, which is the topic of this Deliverable 1.14. Details of the equations and parameters can be found in Appendix B [27].

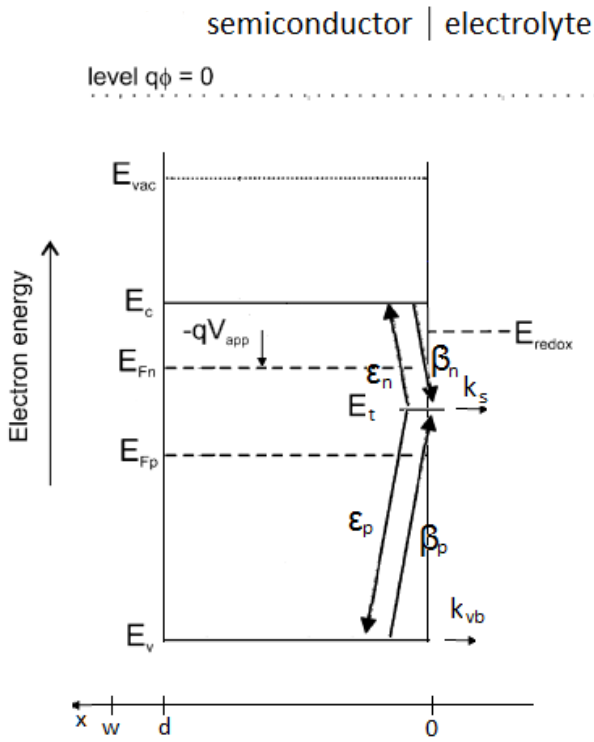

Fig. 16. Scheme of the semiconductor electrolyte interface with surface state kinetics. For simplicity, band bending is not shown.

The established drift-diffusion equations for semiconductor bulk are appended with the transport to and from surface states, Fig. 16. The electrons of the conduction band are trapped with the rate β_n at the discrete surface state with energy E_t and detrapped with the rate ε_n. The holes are transferred with the rate k_{trh} to the electrolyte or trapped with the rate β_p at the surface states, where they are transferred to the electrolyte with the rate k_s or detrapped with the rate ε_p. The occupancy of the trap state is governed by a time-dependent master equation and boundary conditions of our previous model [25] are extended as well. The numerical model was implemented in Comsol Multiphysics and solved for steady-state and transient cases.

The steady-state photocurrent-voltage curves of our model with surface states produces a later photocurrent onset and a flat photocurrent plateau compared to our model without surface states. This shows a monotonic increase of photocurrent without plateau, as can be seen in Fig. 17a. The ideal Gartner photocurrent is also shown for reference. The impedance solution is afterwards found numerically by linear perturbation of the steady-state solution. The effect of an increasing rate constant for surface state charge transfer k_s is shown in Figures 17b-17d. The phase of impedance (Fig. 17c) shows two minima except for k_s=200 s^{-1}. The characteristic lower frequency ≈k_s (marked with arrows) corresponds to rate constant k_s. The second higher characteristic frequency (marked with circles) is related to the recombination lifetime. The absolute value of impedance or equivalently resistance to charge transfer (Fig. 17d) decreases as 1/k_s for low frequencies which is

expected for faster rate constant k_s.

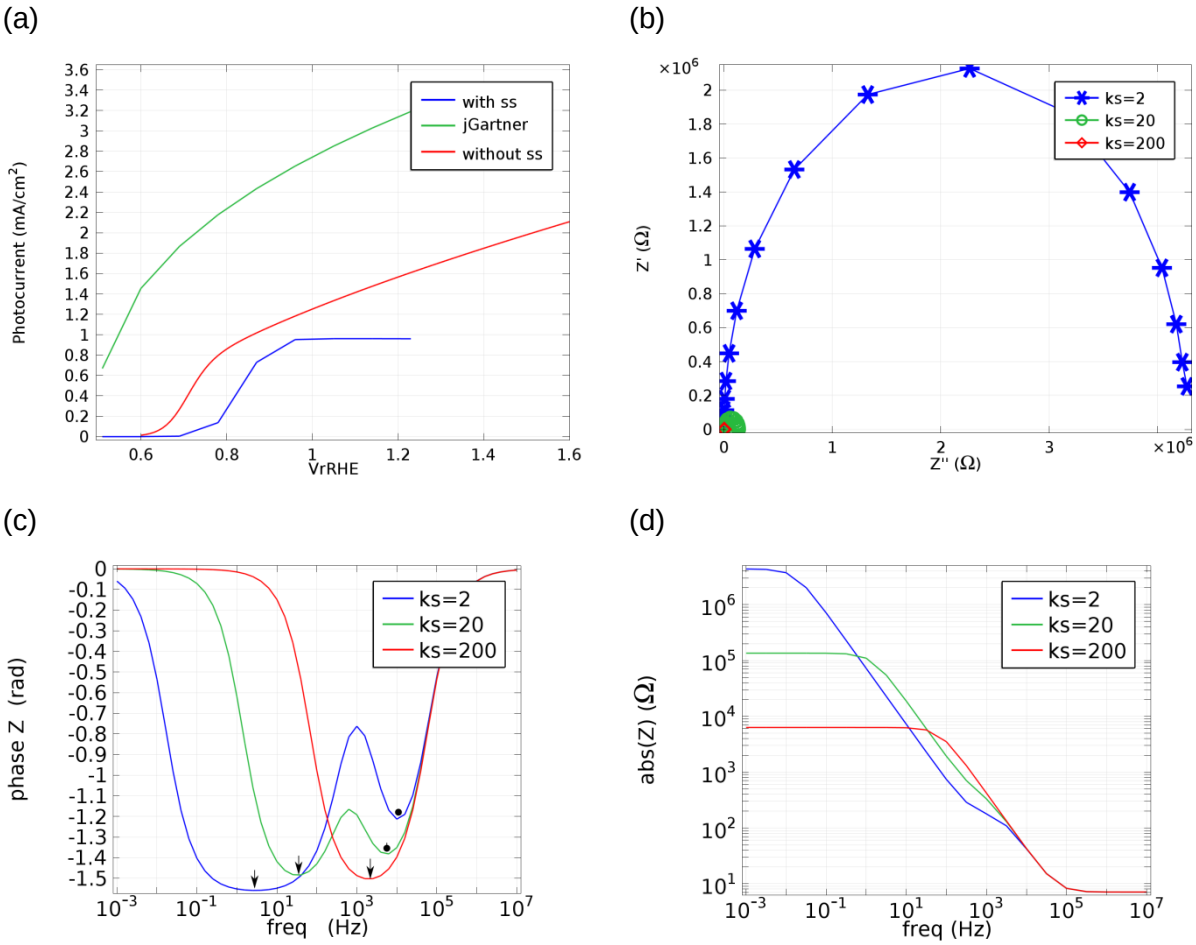

Fig. 17. a) Photocurrent-voltage curves for k_s=20 s^{-1} (with surface states) or k_{trh}=0.1 ms^{-1} (without surface states) and (b-d) impedance simulations of hematite. (b) Nyquist plot (c) Bode phase plot (d) Bode absolute resistance plot.

Our model with surface states represents a solid basis for detailed investigations and validation of different charge transfer kinetics models discussed in the literature. Direct comparison of our simulation with measurements and extraction of the transport parameters from comparison of impedance simulations and measurements are undergoing.

Discussion / appraisal of the results

In 2014 we successfully advanced several PEC concepts, from photoanodes to photocathodes, PEC-PV tandems to photovoltaic-driven systems. We built upon our fundamental knowledge of Fe_2O_3 photoanodes and worked on development of a new synthetic method to realize its full potential. We developed complete water-splitting tandem devices based on Fe_2O_3 and on Cu_2O, and made efforts at scaling them to large dimensions. We achieved great performances in using new materials (CIGS, perovskite) toward water splitting.

We established very high goals at the outset of this project, targeting a highly efficient and stable large scale device. While the target of 10% STH stable for 1000 h on a 100 cm^2 device was not yet fully accomplished, the goal remains a tangible target, for our projects as well as other worldwide

efforts. New developments in CIGS devices point to the possibility of achieving 10% STH in the near future. Our result with perovskite photovoltaics demonstrated that high-performance materials can indeed accomplish solar-to-hydrogen conversion at high efficiency.

For the modeling tasks, in 2014 we completed optical characterization and spectrally-resolved the main optical losses (reflection, transmission) for a test hematite PEC cell at LPI EPFL. We extended the electrical model to account for surface state kinetics. This approach captures qualitatively characteristic frequencies of recombination and water oxidation. The computer software containing the numerical models was developed and is available for LPI EPFL. The validation of our electrical model and extraction of physical parameters from the current project is close to completion.

As stated in the previous sections, our work toward sunlight-driven water splitting continues to stand out in the research field. We have the tools and materials necessary to maintain the competitive advancement of these technologies. The PECHouse2 project involved a variety of topics, fostered numerous national and international collaborations, and led to the publication of many peer-reviewed publications.

Conclusions, outlook, next steps after closure of the project

The PECHouse2 project succeeded in significantly advancing PEC hydrogen production. A summary of the findings, followed by the envisioned follow-up activities, is outlined below:

- Fe_2O_3 requires doping and surface treatments, achievable by underlayers and overlayers, but these conditions are difficult to achieve on the intricate APCVD nanostructures.
    - The ALD deposition of Fe_2O_3 thin films, with doping control and the ability to deposit onto 3D scaffold materials in a host-guest approach, is underway and has been finding success.
- Cu_2O photocathodes can successfully be used in PEC-PV tandems for unassisted water splitting.
    - Compatibility with alkaline solutions is crucial in designing efficient cells, so future research will target making the TiO_2 protective overlayer to be stable in base.
    - Perovskite photovoltaics can lead to efficient PEC-PV tandems with Cu_2O, and can be scaled-up for future integration.
- CIGS represents a material related to Cu_2O that can provide higher performances
    - Further development toward the realization of 10% STH is underway.
- Perovskite photovoltaics can drive water splitting with high efficiency.
    - Further efficiency gains will come from stacked tandems where the perovskite is coupled to, perhaps, Si or CIGS, efforts which are underway.
- Numerical modeling of the PEC photoelectrodes aids understanding limiting factors for commercial PEC hydrogen production
    - Charge transport and efficiency improvements in Cu_2O photocathodes need to be addressed by close interaction of experiments with numerical investigations
    - Coupled optical and electrical modeling is important to understand ways for improvement of the photoelectrodes
    - Large area cells fabricated at EPFL suffer losses which need to be minimized by cell scale modeling
    - PEC-PV tandem performance can be optimized by detailed numerical modeling

The above points represent current and future work, which will be proposed for the continuation of PECHouse in a new project PECHouse3. Meanwhile, our group is participating in related ongoing

projects including PECDEMO (EU) and TANDEM (Nano-Tera). With these continued efforts we aim to develop commercially-viable PEC-based solar fuels devices.

References

Legend: PECHouse2 publications

1. Paracchino, A. *et al.* Ultrathin films on copper(i) oxide water splitting photocathodes: a study on performance and stability. *Energy Environ. Sci.* **5,** 8673 (2012).

2. Tilley, S. D., Cornuz, M., Sivula, K. & Grätzel, M. Light-Induced Water Splitting with Hematite: Improved Nanostructure and Iridium Oxide Catalysis. *Angew. Chemie* **122,** 6549–6552 (2010).

3. Cesar, I., Kay, A., Gonzalez Martinez, J. a & Grätzel, M. Translucent thin film Fe2O3 photoanodes for efficient water splitting by sunlight: nanostructure-directing effect of Si-doping. *J. Am. Chem. Soc.* **128,** 4582–3 (2006).

4. Steier, L. *et al.* Understanding the Role of Underlayers and Overlayers in Thin Film Hematite Photoanodes. *Adv. Funct. Mater.* **24,** 7681–7688 (2014).

5. Warren, S. C. *et al.* Identifying champion nanostructures for solar water-splitting. *Nat. Mater.* **12,** 842–9 (2013).

6. Hisatomi, T. *et al.* Cathodic shift in onset potential of solar oxygen evolution on hematite by 13-group oxide overlayers. *Energy Environ. Sci.* **4,** 2512 (2011).

7. Hisatomi, T. *et al.* Enhancement in the performance of ultrathin hematite photoanode for water splitting by an oxide underlayer. *Adv. Mater.* **24,** 2699–702 (2012).

8. Hisatomi, T. *et al.* A Ga2O3 underlayer as an isomorphic template for ultrathin hematite films toward efficient photoelectrochemical water splitting. *Faraday Discuss.* **155,** 223 (2012).

9. Morales-Guio, C. G. *et al.* An Optically Transparent Iron Nickel Oxide Catalyst for Unassisted Solar Water Splitting on a Stacked Hematite-Perovskite Tandem Cell. *(submitted)*

10. Brillet, J. *et al.* Highly efficient water splitting by a dual-absorber tandem cell. *Nat. Photonics* **6,** 824–828 (2012).

11. Azevedo, J. *et al.* On the stability enhancement of cuprous oxide water splitting photocathodes by low temperature steam annealing. *Energy Environ. Sci.* Advance Article (2014). doi:10.1039/C4EE02160F

12. Seger, B. *et al.* Silicon protected with atomic layer deposited TiO2: conducting versus tunnelling through TiO2. *J. Mater. Chem. A* **1,** 15089 (2013).

13. Seger, B. *et al.* Silicon protected with atomic layer deposited TiO2: durability studies of photocathodic H2 evolution. *RSC Adv.* **3,** 25902 (2013).

14. Hu, S. *et al.* Amorphous TiO2 coatings stabilize Si, GaAs, and GaP photoanodes for efficient water oxidation. *Science* **344,** 1005–9 (2014).

15. Tilley, S. D., Schreier, M., Azevedo, J., Stefik, M. & Grätzel, M. Ruthenium Oxide Hydrogen Evolution Catalysis on Composite Cuprous Oxide Water-Splitting Photocathodes. *Adv. Funct. Mater.* **24,** 303–311 (2014).

16. Morales-Guio, C. G., Tilley, S. D., Vrubel, H., Grätzel, M. & Hu, X. Hydrogen evolution from a copper(I) oxide photocathode coated with an amorphous molybdenum sulphide catalyst. *Nat. Commun.* **5,** 3059 (2014).

17. Mayer, M. T. *et al.* Transparent Cu2O photocathodes in tandem with perovskite photovoltaics enabling complete water splitting. *(in Prep.* (2015).

18. Morales-Guio, C. G. *et al.* Photoelectrochemical Hydrogen Production in Alkaline Solutions Using Cu2 O Coated with Earth-Abundant Hydrogen Evolution Catalysts. *Angew. Chem. Int. Ed. Engl.* 1–5 (2014). doi:10.1002/anie.201410569

19. Marshall, J. Solar energy: Springtime for the artificial leaf. *Nature* **510,** 22–4 (2014).

20. Luo, J. *et al.* Water photolysis at 12.3% efficiency via perovskite photovoltaics and Earth-abundant catalysts. *Science* **345,** 1593–1596 (2014).

21. Khaselev, O., Bansal, A. & Turner, J. A. High-efficiency integrated multijunction photovoltaic/electrolysis systems for hydrogen production. *Int. J. Hydrogen Energy* **26,** 127–132 (2001).

22. Cox, C. R., Lee, J. Z., Nocera, D. G. & Buonassisi, T. Ten-percent solar-to-fuel conversion with nonprecious materials. *Proc. Natl. Acad. Sci.* 1–5 (2014). doi:10.1073/pnas.1414290111

23. Bailie, C. D. *et al.* Polycrystalline Tandem Photovoltaics Using Perovskites on Top of Silicon and CIGS. *Energy Environ. Sci.* (2014). doi:10.1039/C4EE03322A

24. Bisquert, J., Cendula P., Bertoluzzi L., Gimenez, S. Energy diagram of semiconductor-electrolyte junctions. *J. Phys. Chem. Lett. 2014, 205–207.*

25. Cendula, P.; Tilley, S. D.; Gimenez, S.; Schmid, M.; Bisquert, J.; Graetzel, M.; Schumacher, J. O. Calculation of the Energy Band Diagram of a Photoelectrochemical Water Splitting Cell, Journal of Physical Chemistry C 2014, 118, 29599–29607.

26. Cendula, P.; Steier, L., Tilley, S. D.; Mayer, M. T.; Schmid, M.; Graetzel, M.; Schumacher, J. O. Quantitative Analysis of Optical Losses in Hematite Photoelectro-chemical Cell, (In preparation) 2015.

27. Cendula, P.; Jarolin, M., Tilley, S. D.; Mayer, M. T; Graetzel, M.; Schumacher, J. O. Determination of rate constants for hematite photoelectrodes from drift-diffusion model with surface states, (In preparation) 2015.

Appendix A: Manuscript of Ref. 26

Appendix B: Ref. 27